

# Primordial black holes and Scalar-Induced Gravitational Waves formed by inflation potential with non-trivial characteristics

Ruifeng Zheng\* and Yanqing Xu

Physics Department, College of Physics and Optoelectronic Engineering, Jinan University, Guangzhou 510632, China

The formation of primordial black holes (PBHs) generally requires large density perturbations, which is widely supported by researchers. This paper studies the local coupling properties of the Starobinsky potential and KKLT potential by introducing a linear Lorentzian-type coupling, which locally breaks the slow roll conditions. We found that both positive and negative coupling can form a considerable abundance of PBH. Additionally, we also studied the scalar-induced gravitational waves (SIGWs) generated by this model.

## I. INTRODUCTION

Black holes, as one of the most extreme predictions of Einstein's theory of general relativity, have long inspired humanity to explore the deepest mysteries of the universe. Conventionally, black holes are understood to form primarily through the gravitational collapse of massive stellar cores (typically exceeding 20–25 solar masses) during supernova explosions at the end of stellar evolution, or via the merger and accretion of stellar-mass or intermediate-mass black holes. However, within the extreme high-energy conditions prevalent in the very early universe, a distinct class of black holes with an alternative origin may exist: Primordial Black Holes (PBHs). These types of black holes do not originate from the death of stars, but are directly born from the strong non-uniformity of energy distribution (density disturbance) in the very early universe (usually within about 1 second after the Big Bang). Their formation mechanism is thus decoupled from standard stellar evolution. Theoretically, PBHs can possess mass spectra spanning an extraordinarily wide range, from subatomic scales ( $\sim 10^{-5}g$ ) to supermassive ranges ( $> 10^5 M_\odot$ ) and beyond.

The PBHs were first systematically proposed by Hawking [1, 2] and Zeldovich [3] in the 1960s and 1970s. The core formation mechanism posits that during the radiation-dominated epoch immediately following inflation, if the density perturbation amplitude of certain spatial regions is large enough to exceed the critical value ( $\delta > \delta_c$ ), so that their self-gravity overcomes the cosmic expansion and radiation pressure, then these regions will undergo direct gravitational collapse, skipping the long process of star formation and directly forming black holes. This gravitational collapse is thought to occur when the cosmic age  $t < 1s$ . Consequently, PBH formation depends critically on the spectral characteristics of primordial density perturbations in the early-universe, particularly at small scales. The origin of these perturbations is usually closely related to the details of inflation models, cosmic phase transitions (such as QCD phase transitions), the generation of cosmic strings or other

topological defects, and the evolution of scalar fields. Therefore, various PBHs formation mechanisms has been proposed [4–23].

PBHs within certain mass ranges are regarded as plausible candidates for dark matter. If they constitute all or a significant part of dark matter, this could offer new perspectives on the fundamental properties of dark matter, avoiding the dilemma of traditional weakly interacting massive particles (WIMPs) waiting to be selected as particles that have not yet been discovered in direct detection and accelerator experiments. However, as one of the candidates for dark matter, PBHs are not without challenges. Various astronomical observations and cosmological limitations, such as the cosmic microwave background (CMB) and big bang nucleosynthesis (BBN) [24–26], BH evaporation [27], Gravitational-Wave Lensing (GW-Lensing) [28], gamma-ray emission [29–32], gravitational waves [33–35] and so on, impose strict constraints on PBHs as dark matter candidates or their abundance in different mass ranges. These constraints indicate that if PBHs exist, they are unlikely to dominate dark matter in all mass ranges. However, they may plausibly constitute either the entirety or a substantial fraction of dark matter within specific, currently observationally viable mass windows, or exist as a subcomponent of dark matter.

Ultra-slow-roll (USR) inflation is considered as one of the effective mechanisms for the formation of PBHs [4, 36], a viable USR model must simultaneously satisfy large-scale cosmological observational constraints while significantly amplifying the primordial power spectrum at small scales. In addition, large scalar perturbations may contribute to the generation of Scalar-Induced Gravitational Waves (SIGWs) [37–39], which further limits the degree of amplitude enhancement of the primordial power spectrum during inflation.

In this paper, we study a toy inflation model characterized by the local coupling of the basic inflation potential with the Lorentz function. This special mechanism of locally coupled dynamic adjustment allows the equation of motion for the scalar field to transition from conventional slow-roll (SR) inflation to USR inflation over a period of time. The SR parameters exhibit exponential changes, leading to a sharp increase in the power spectrum and could potentially satisfy PBHs formation requirements. Our results indicate that regardless of whether the cou-

\* zrf2022@stu2022.jnu.edu.cn

pling is positive or negative, both lead to a significant enhancement of the power spectrum on small scales.

This paper is organized as follows. In Sec. II, we briefly review the relevant details of SR inflation and USR inflation. In Sec. III, we introduce the Starobinsky potential and KKLT potential with a locally coupled form; the derived power spectrum satisfies the observational constraints from the CMB on large scales while exhibiting enhanced peaks on small scales. In Sec. IV, we calculate the abundance of PBHs formed by our model. In Sec. V, we discuss the SIGWs generated by scalar perturbations and In Sec. VI, we present our conclusions and discussions. In the appendix, we also provide a simple extension to this method.

## II. SR AND USR OF SCALAR FIELD

The action of a single scalar field inflation model is usually given by

$$S = \int d^4x \sqrt{-g} \left[ \frac{M_{pl}^2 R}{2} - \frac{1}{2} \partial_\mu \phi \partial^\mu \phi - V(\phi) \right], \quad (1)$$

where  $R$  is the Ricci scalar,  $V(\phi)$  is the inflation potential, the corresponding Friedman equation and the equation of motion of scalar field can be written as

$$\begin{aligned} H^2 &= \frac{1}{3M_{pl}^2} \left( \frac{1}{2} \dot{\phi}^2 + V(\phi) \right), \\ \ddot{\phi} + 3H\dot{\phi} + V'(\phi) &= 0, \end{aligned} \quad (2)$$

where  $H$  is the Hubble parameter,  $\dot{\phi} = d\phi/dt$ , in order to describe the process of inflation, the SR parameter is usually defined as

$$\begin{aligned} \epsilon_H &= -\frac{\dot{H}}{H^2}, \\ \eta_H &= -\frac{\ddot{H}}{2\dot{H}H}, \\ \xi_H &= \frac{\ddot{H}}{2H^2\dot{H}} - 2\eta_H^2. \end{aligned} \quad (3)$$

The SR inflation requires that the values of the SR parameters mentioned above be  $\ll 1$  during inflation. In addition, in order to solve the problem of the Big Bang, the e-foldings number is required [40]

$$N \equiv N_i - N_e = \int_{t_i}^{t_e} H(t) dt \geq 60. \quad (4)$$

Now let's discuss the perturbations generated during inflation, under the FRW metric, we define the Mukhanov-Sasaki(MS) variable as  $u \equiv z\zeta$ ,  $z \equiv a\dot{\phi}/H$  and the variable satisfies the Mukhanov-Sasaki equation [41, 42]

$$u''_k + \left( k^2 - \frac{z''}{z} \right) u_k = 0, \quad (5)$$

the prime denotes the derivative with respect to comoving time  $\tau$ , and the effective potential term is given by

$$\begin{aligned} \frac{z''}{z} &= 2a^2 H^2 \left( 1 + \epsilon_H - \frac{3}{2} \eta_H + \epsilon_H^2 \right. \\ &\quad \left. + \frac{1}{2} \eta_H^2 - 2\epsilon_H \eta_H + \frac{1}{2} \xi_H \right), \end{aligned} \quad (6)$$

where  $a$  is the scale factor. By solving Eq. (5) and adopting the relationship between the MS variable and its dimensionless primordial power-spectrum [5], we get

$$P_S = \frac{k^3}{2\pi^2} \frac{|u_k|^2}{z^2} \Big|_{k \ll aH}. \quad (7)$$

In addition, we can obtain the perturbation power spectrum under the SR approximation as

$$P_S = \frac{1}{8\pi^2 \epsilon_H} \left( \frac{H}{M_{pl}} \right)^2. \quad (8)$$

Large scale observations indicate that the primordial power spectrum has near scale invariant, which means the scalar spectral tilt [43]

$$n_s = 1 + 2\eta_H - 4\epsilon_H \sim 0.968, \quad (9)$$

and the tensor-to-scalar ratio

$$r \approx 16\epsilon_H < 0.03. \quad (10)$$

Planck 2018 observations constrain the amplitude of the power spectrum to approximately  $\sim 10^{-9}$  [43]. However, this is not conducive to the formation of PBHs. In order to form a sufficient number of PBHs, the power spectrum needs to be increased to at least  $\sim 10^{-2}$  on small scale [44]. A reasonable way is to locally break this SR state, which corresponds to the USR state. In the USR state, the equation of motion of the scalar field is rewritten as [45, 46]

$$\ddot{\phi} + 3H\dot{\phi} = -V'(\phi) = 0, \quad (11)$$

which means the SR parameter  $\epsilon_H$  will decay exponentially. According to Eq. (8), this leads to an exponential growth of the power spectrum. It is important to note that this evolution disrupts the slow-roll condition, causing the parameter  $\eta_H = 3 + \epsilon_H$  to exceed 1 [47]. As a result, the SR approximation breaks down and the system enters a phase of USR inflation. However, this is only temporary. When the evolution of the scalar field deviates from the local coupling of potential, the system will resume SR inflation again and continue until the inflation ends.

## III. LOCAL COUPLED INFLATION POTENTIAL

The SR inflationary scenario can successfully account for current observational constraints, such as the scalar

spectral index  $n_s \approx 0.968$  and the tensor-to-scalar ratio  $r < 0.03$ . In order to achieve USR inflation, one approach is to propose a new USR inflation potential that conforms to various parameter constraints given by the SR approximation on large scale, which requires us to consider the inflation potential globally [4], or adopt a simpler approach based on introducing a local feature into a known SR potential. The latter method can temporarily violate SR conditions on small scales while remaining consistent with large-scale observations.

Here, we introduce a method for realizing localized modifications by coupling a Lorentzian function to the potential. This coupling induces inflection points at suitable locations, leading to a pronounced peak in the power spectrum on small scales. It is worth emphasizing that this new inflection point method is universal, and in principle, it can be locally coupled to any inflation potential without significantly affecting large-scale observation constraints. In this paper, firstly, we adopt the Starobinsky potential as the basic potential [48], the full form of the potential is given by

$$V(\phi) = V_0 \left(1 - e^{A_1 \phi}\right)^2 \left(1 \pm \frac{B_1 C_1}{(\phi - D_1)^2 + C_1^2}\right), \quad (12)$$

where  $V_0$  fixes the overall CMB normalization and  $A_1, B_1, C_1, D_1$  represents the relevant parameters. Specifically,  $A_1$  determines the specific form of the basic potential function, and  $B_1, C_1, D_1$  represents the position, width, and amplitude of coupling, respectively. The "+" indicates positive coupling, and "-" indicates negative coupling. In order to satisfy the constraints of large-scale observations, we choose  $V_0 = 10^{-10} M_{pl}^4$ ,  $A_1 = -0.8165 M_{pl}^{-1}$ , the initial value of the scalar field is set to  $\phi_i = 5.4 M_{pl}$ , which conforms to the constraints of current cosmological observations

$$\begin{aligned} n_s &= 0.966338, \\ r &= 0.00323652. \end{aligned} \quad (13)$$

Although the coupling term can also affect the above two parameters, it should be noted that the effect of the coupling term only appears locally in the potential, which doesn't affect the initial value of the field. Therefore, the impact on the large scale can be almost negligible.

Firstly, we consider positive coupling "+" with the following parameter values

$$\begin{aligned} B_1 &= 6.23278 \cdot 10^{-5} M_{pl}, \\ C_1 &= 0.025 M_{pl}, \\ D_1 &= 4 M_{pl}. \end{aligned} \quad (14)$$

The potential is shown in Fig.(1), we can see that the effect of positive coupling is reflected in  $\phi = 4 M_{pl}$ , manifesting as a local bumpy of potential, this creates a locally flat range of potential. The width and height of the bump directly affect the peak of the power spectrum, and ultimately affect the abundance of the PBHs formed.

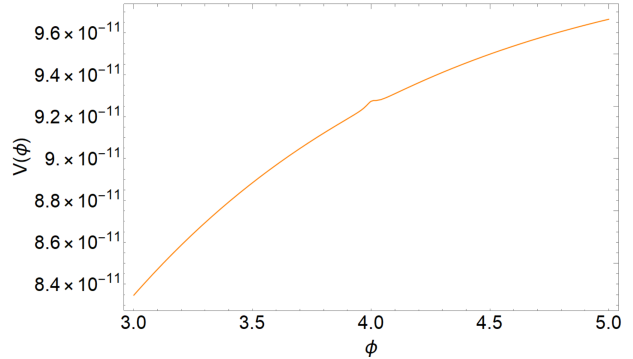


FIG. 1. The Starobinsky potential with local positive coupling corresponds to Eq. (12), and the parameter values correspond to Eq. (14), where the coupling is at  $\phi = 4 M_{pl}$  and the initial value of the scalar field is at  $\phi_i = 5.4 M_{pl}$ . The vast range of potentials outside the coupling still satisfies SR inflation.

Therefore, detailed adjustment of parameters is required.

As shown in Fig. (2), by solving the equation of motion (2) of the scalar field  $\phi$ , we can obtain the evolution curve of the scalar field with respect to the e-foldings number  $N$ . Due to local coupling, the SR condition of the scalar field is broken locally. The motion of the scalar field at this coupling point is extremely slow and the system transitions from SR inflation to USR inflation.

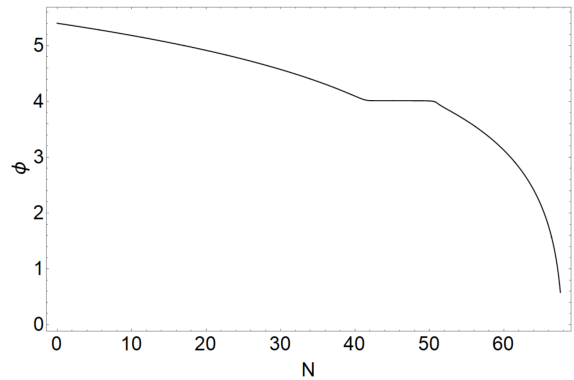


FIG. 2. The figure shows the evolution of the scalar field  $\phi$  of the local positive coupling form of the Starobinsky potential with respect to the e-foldings number  $N$ . Around  $N \approx 45$ , the system transitions from SR inflation to USR inflation.

The existence of coupling causes significant changes in the evolution of SR parameters  $\epsilon_H$  and  $\eta_H$  locally. From Fig. (3) and Fig. (4), it can be seen that  $\epsilon_H$  sharply decreases near  $N \approx 45$ , while  $\eta_H$  shows an increasing trend and dynamically breaks the SR state  $\eta_H > 1$ , which is precisely one of the characteristics of USR inflation. However, this does not mean the end of inflation. Afterwards, when the scalar field successfully passes through the coupling point, it will return to the SR state, and re-satisfy the SR condition  $\epsilon_H, \eta_H < 1$ , and eventually end

inflation at  $N \approx 67$ .

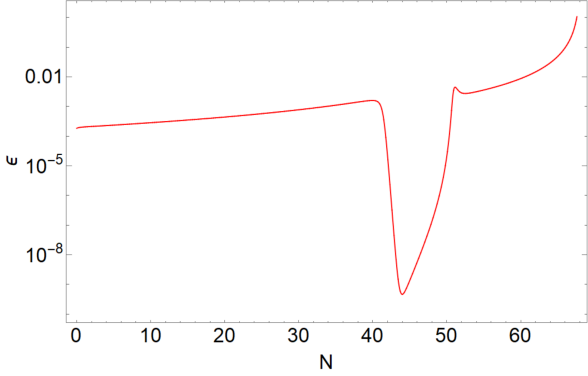


FIG. 3. The figure shows the evolution of the SR parameter  $\epsilon_H$  of the local positive coupling form of the Starobinsky potential with the e-foldings number  $N$ , and at  $N \approx 45$ ,  $\epsilon_H$  shows a sharp downward trend.

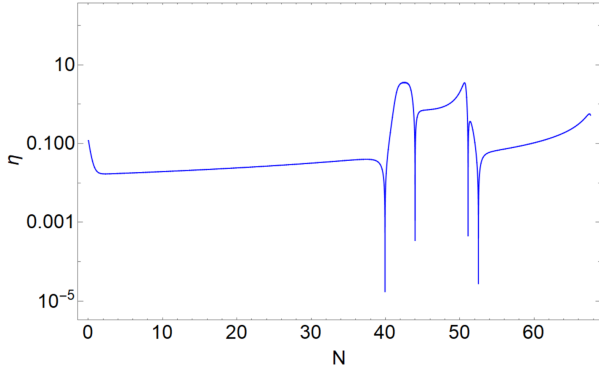


FIG. 4. The figure shows the evolution of the SR parameter  $\eta_H$  of the local positive coupling form of the Starobinsky potential with the e-foldings number  $N$ , where  $\eta_H$  temporarily breaks the SR condition at  $N \approx 45$ .

By numerically solving the MS equation (5), we obtained the variation of the power spectrum (7) with wave number  $k$ . From Fig. (5), it can be seen that on large scale, our model satisfies the observation constraints of CMB ( $\sim 10^{-9}$ ), and on small scale with  $k \sim 10^{17} \text{Mpc}^{-1}$ , there is a peak ( $\sim 10^{-2}$ ) in the power spectrum.

In addition to positive coupling that can enhance small-scale power spectrum, we will show that negative coupling can also achieve the same effect. Negative coupling indicates that in Eq. (12), the coupling term is  $-B_2 C_2 / ((\phi - D_2)^2 + C_2^2)$ , the relevant parameters are as follows

$$\begin{aligned} B_2 &= 5.6775 \cdot 10^{-5} M_{pl} , \\ C_2 &= 0.025 M_{pl} , \\ D_2 &= 4.4 M_{pl} . \end{aligned} \quad (15)$$

In Fig. (6), we have plotted the potential curve with negative coupling. The negative coupling is located at

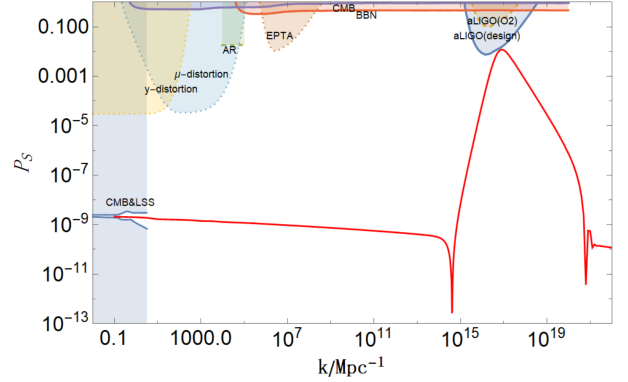


FIG. 5. The relationship between power spectrum with positive coupling form of Starobinsky potential and wave number  $k$ , where the observation of CMB is satisfied on large scale, but there is a significant improvement in power spectrum on small scale, the color region is excluded by the current observation.

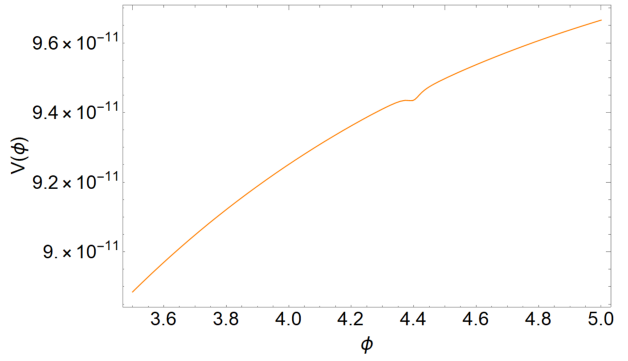


FIG. 6. The Starobinsky potential with negative coupling, and the parameter values correspond to Eq. (15), where the coupling is at  $\phi = 4.4 M_{pl}$  and the initial value of the scalar field is at  $\phi_i = 5.4 M_{pl}$ . The vast range of potentials outside the coupling still satisfies SR inflation.

$\phi = 4.4 M_{pl}$ , specifically corresponding to a local dip in the potential curve.

Similarly, by solving the equation of motion (2) of scalar field, we can obtain the evolution curve of the scalar field with negatively coupled form. From Fig. (7), we can easily see that near  $N \approx 35$ , the evolution of the scalar field  $\phi$  transitions from the SR state to USR state, manifested by an extremely low slope. This means that compared to Fig. (2), negative coupling achieves a similar effect as positive coupling.

The influence of negative coupling on the SR parameters  $\epsilon_H$  and  $\eta_H$  is shown in Fig. (8) and Fig. (9). We can see that  $\epsilon_H$  decreases significantly near  $N \approx 35$ , while  $\eta_H$  temporarily breaks the SR condition. When the scalar field evolves beyond negative coupling,  $\epsilon_H$  and  $\eta_H$  satisfy the SR condition again  $\epsilon_H, \eta_H < 1$  and end inflation near  $N \approx 65$ .

In Fig. (10), we obtained the power spectrum in negative coupling form, which satisfies the observation con-

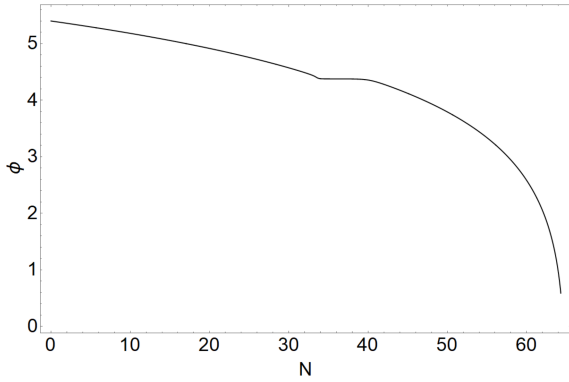


FIG. 7. The figure shows the evolution of the scalar field  $\phi$  of the local negative coupling form of the Starobinsky potential with respect to the e-foldings number  $N$ . Around  $N \approx 35$ , the system transitions from SR inflation to USR inflation.

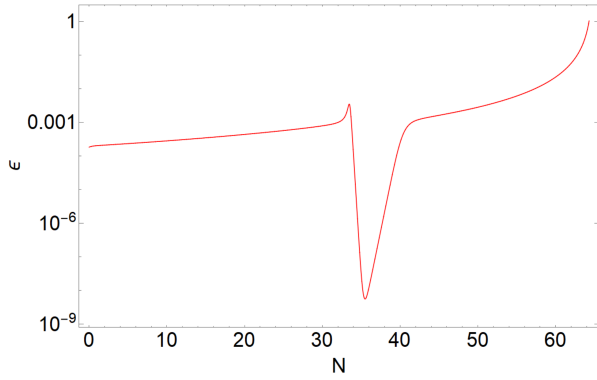


FIG. 8. The figure shows the evolution of the SR parameter  $\epsilon_H$  of the local negative coupling form of the Starobinsky potential with the e-folding number  $N$ , and at  $N \approx 35$ ,  $\epsilon_H$  shows a sharp downward trend.

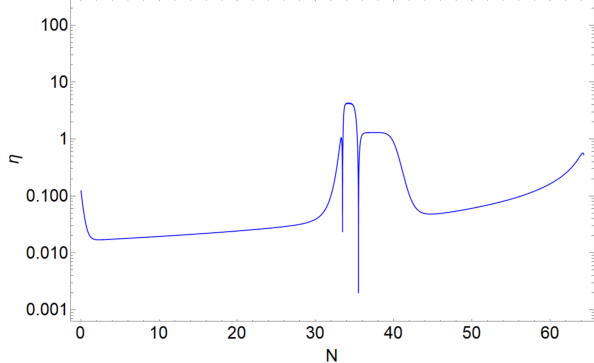


FIG. 9. The figure shows the evolution of the SR parameter  $\eta_H$  of the local negative coupling form of the Starobinsky potential with the e-folding number  $N$ , where  $\eta_H$  temporarily breaks the SR condition at  $N \approx 35$ .

straints of CMB on large scale ( $\sim 10^{-9}$ ), but exhibits a peak ( $\sim 10^{-2}$ ) at  $k \sim 10^{13} \text{Mpc}^{-1}$  on small scale.

In order to demonstrate the universality of this method, we take the KKLT inflation potential [49, 50] as

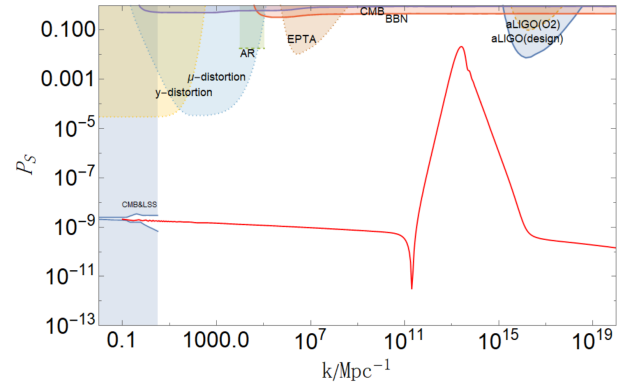


FIG. 10. The relationship between power spectrum with negative coupling form of Starobinsky potential and wave number  $k$ , where the observation of CMB is satisfied on a large scale, but there is a significant improvement in power spectrum on a small scale, and the color region is excluded by the current observation.

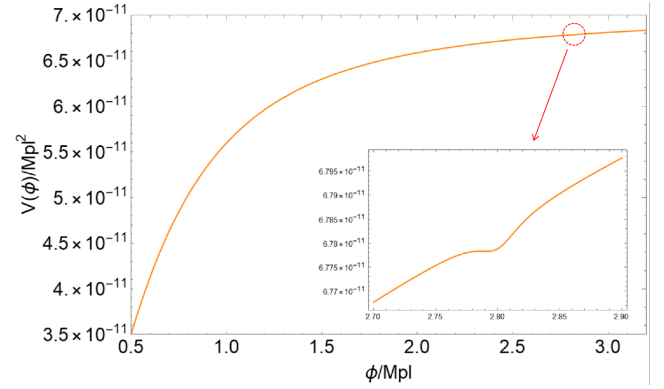


FIG. 11. The KKLT potential with negative coupling, and the parameter values correspond to Eq. (17), where the coupling is at  $\phi = 2.8M_{pl}$ .

an example. Through local negative coupling, the complete KKLT inflation potential is

$$V(\phi) = V_3 \frac{\phi^2}{\phi^2 + 1/4} \left( 1 - \frac{B_3 C_3}{(\phi - D_3)^2 + C_3^2} \right), \quad (16)$$

where  $V_3 = 7 \cdot 10^{-11} M_{pl}^4$ , the initial value of the scalar field is set to  $\phi_i = 3.1 M_{pl}$ , which conforms to the constraints of current cosmological observations. the relevant parameters are as follows

$$\begin{aligned} B_3 &= 1.4275 \cdot 10^{-5} M_{pl}, \\ C_3 &= 0.02 M_{pl}, \\ D_3 &= 2.8 M_{pl}. \end{aligned} \quad (17)$$

The potential is shown in Fig.(16), we can see that the effect of negative coupling is reflected in  $\phi = 2.8M_{pl}$ . In Fig.(12), we plot the evolution of the SR parameters  $\epsilon_H$  and  $\eta_H$  of the KKLT potential in the form of local negative coupling. Around  $N \approx 15$ , the system transitions from SR to USR. The power spectrum formed by

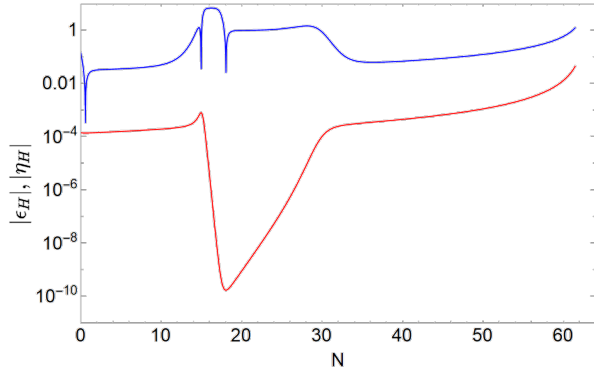


FIG. 12. Evolution curve of KKLT SR parameters, the blue line corresponding to  $\eta_H$  and the red line corresponding to  $\epsilon_H$ .

KKLT in the form of local negative coupling is shown in Fig. (13), we can see a peak in the power spectrum at  $k \sim 2.3 \cdot 10^5 \text{Mpc}^{-1}$ . This indicates that this locally

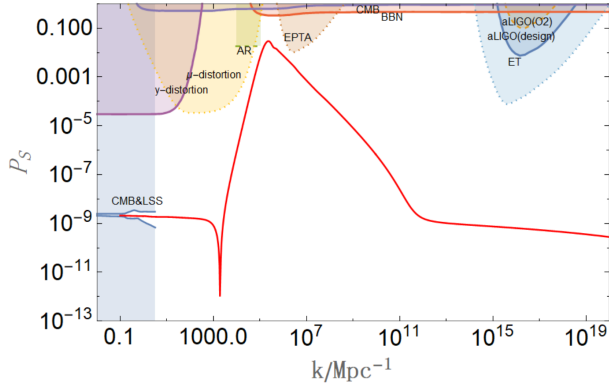


FIG. 13. The power spectrum formed by KKLT with local negative coupling.

coupled method can be easily extended to other inflation potential that conform to current observations.

#### IV. PBH ABUNDANCE

Due to gravitational collapse, if the fluctuations re-entering the horizon are large enough, PBHs with a wide range of masses may form. The mass of PBHs formed during the radiation-dominated period is equivalent to the Hubble mass during that period [51, 52]

$$M_{PBH} = \gamma M_H = \gamma \sqrt{\frac{2\pi}{3G}} \rho_{\text{form}}^{1/2} H_{\text{form}}^{-2} , \quad (18)$$

where  $\gamma \simeq 0.2$  is the efficiency factor,  $\rho_{\text{form}}$  and  $H_{\text{form}}^{-1}$  represent the Hubble radius and the energy density of the universe respectively. In addition, in order to calculate the abundance of PBHs of specific mass and relate it to the power spectrum, we usually express the PBH mass

and the  $k_{\text{form}}$  as [53]

$$M_{PBH} = 2 \cdot 10^{48} \left( \frac{\gamma}{0.2} \right) \left( \frac{g_*}{106.75} \right)^{-\frac{1}{6}} \left( \frac{k_{\text{form}}}{0.07 \text{Mpc}^{-1}} \right)^{-2} g , \quad (19)$$

where  $g_*$  is the total effective degree of freedom of the universe in the radiation dominated era. This means that for a given  $k_{\text{form}}$ , we can obtain the corresponding  $M_{PBH}$ .

To evaluate the proportion of PBHs as dark matter, the abundance of PBHs is typically defined as [25]

$$\begin{aligned} f_{PBH} &= \frac{\rho_{PBH}}{\rho_{DM}} |_{\text{form}} \\ &= 1.68 \cdot 10^8 \left( \frac{\gamma}{0.2} \right)^{\frac{1}{2}} \left( \frac{g_*}{106.75} \right)^{-\frac{1}{4}} \\ &\quad \times \left( \frac{M_{PBH}}{M_\odot} \right)^{-\frac{1}{2}} \beta(M_{PBH}) , \end{aligned} \quad (20)$$

where the collapse fraction  $\beta(M_{PBH}) = \rho_{PBH}/\rho_{DM}$  is the fraction of PBHs in the entire universe when it is formed, the standard treatment method for  $\beta(M)$  is based on Press-Schechter formalism [54, 55]. For Gaussian primordial fluctuations,  $\beta(M)$  is given by [56, 57]

$$\begin{aligned} \beta(M(k)) &= 2 \int_{\delta_c}^{\infty} \exp \left( -\frac{\delta^2}{2\sigma^2(M(k))} \right) \frac{d\delta}{\sqrt{2\pi}\sigma(M(k))} \\ &= \sqrt{\frac{2}{\pi}} \frac{\sigma(M(k))}{\delta_c} \exp \left( -\frac{\delta_c^2}{2\sigma^2(M(k))} \right) , \end{aligned} \quad (21)$$

where  $\delta_c$  is the threshold density, in the radiation period, some studies have shown that the threshold density may be between  $0.33 - 0.66$  [58, 59], which means that the collapse fraction will be uniquely determined by the variance  $\sigma^2(M(k))$  [60, 61]

$$\sigma^2(M(k)) = \frac{16}{81} \int_0^\infty d\ln q \left( \frac{q}{k} \right)^4 W \left( \frac{q}{k} \right)^2 P_S(q) , \quad (22)$$

where  $P_S(q)$  is the power spectrum of curvature perturbation and  $W(x)$  is the smooth window function [62, 63], here, we have adopted the most commonly used Gaussian form  $W(x) = \exp(-x^2/2)$ .

In Fig. (14), we obtain the numerical solution for the abundance of PBHs formed by positive coupling, where  $k_{\text{form}} = 8.318 \cdot 10^{16} \text{Mpc}^{-1}$  and the corresponding PBH mass is  $M_{PBH} = 5.319 \cdot 10^{-22} M_\odot$ . We separately plotted the effects of different threshold densities on the abundance of PBHs. The results have shown that the abundance of PBHs is inversely proportional to the threshold density. The numerical results indicate that when the threshold density is  $\delta_c = 0.35$ , the abundance of PBHs is approximately  $2.9 \cdot 10^{-5}$ , which corresponds to the upper limit of the abundance of PBH predicted by BBN [27]. It should be noted that due to Hawking radiation, PBHs with initial mass of less than  $10^{15} g$  have now evaporated and cannot constitute current dark matter. However, small-mass black holes will emit a large number of particles due to Hawking radiation [64], which may have a

significant impact on the early universe's BBN. The impact on BBN is the subject of future work and will not be further analyzed here.

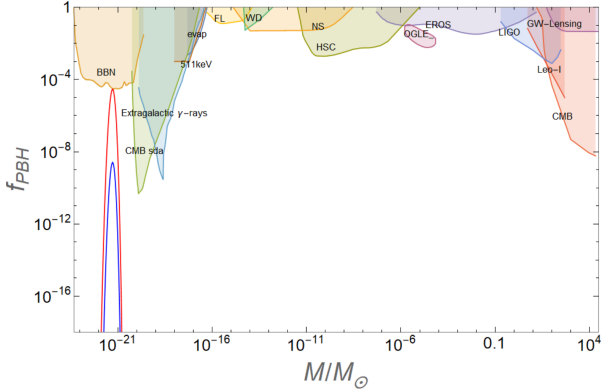


FIG. 14. The figure shows the abundance of PBHs formed by the Starobinsky potential with positive coupling, where the blue line corresponding to the threshold density is  $\delta_c = 0.38$  and the red line corresponding to the  $\delta_c = 0.35$ . Different color ranges are excluded by current observations, and our results conform to the constraints of current observations. Constraints are obtained from the publicly available Python code PBHbounds [65].

Negative coupling can also lead to a significant enhancement of the power spectrum on small scales, which consequently facilitates the production of PBHs. In Fig. (15), we numerically solved the abundance of PBHs formed by Starobinsky potential with negative coupling form, the plot reveals that at wavenumber  $k = 2.57 \cdot 10^{13} \text{Mpc}^{-1}$  and the corresponding PBH mass is  $M_{PBH} = 5.57 \cdot 10^{-15} M_\odot$ . This mass corresponds to the PBH within the mass range of asteroids, the constraint within this mass range is WD [66], FL [67], NS [68]. The PBH abundance reaches 0.01 when the threshold density is  $\delta_c = 0.4$ . Naturally, a slight lowering of the threshold density would further increase the PBH abundance.

This means that whether it is positive or negative coupling, the Starobinsky potential of locally coupled Lorentz functions may form PBHs without violating the current observation constraints. In addition, in Fig. (16), we plotted the PBHs abundance formed by KKLT potential with local negative coupling form, and the corresponding PBH mass is  $M_{PBH} \approx 70 M_\odot$ , this may be related to the gravitational wave signals observed by LIGO.

## V. SCALAR-INDUCED GRAVITATIONAL WAVES

Large scale primordial scalar perturbations on a small scale can not only form primordial black holes, but also induce the generation of gravitational waves through second-order effects [37, 38], which may be detected by current detectors. Therefore, it has become another im-

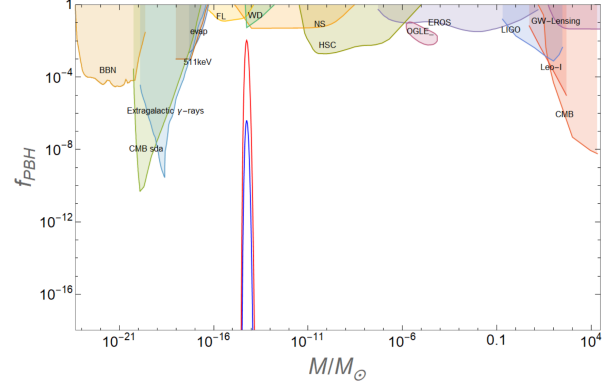


FIG. 15. We plot the abundance of PBHs formed by the Starobinsky potential with negative coupling, where the blue line corresponding to the threshold density is  $\delta_c = 0.45$  and the red line corresponding to the  $\delta_c = 0.4$ . Our results conform to the constraints of current observations. Constraints are obtained from the publicly available Python code PBHbounds [65].

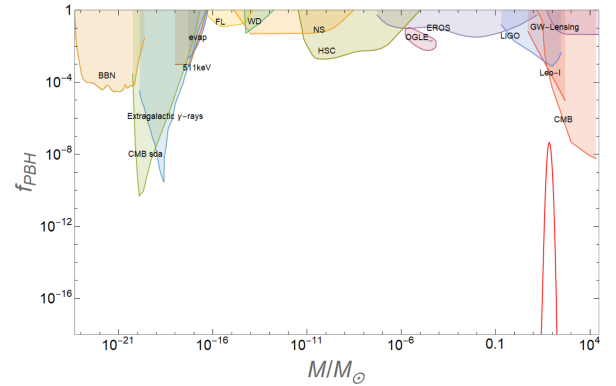


FIG. 16. The abundance of PBHs formed by KKLT potentials with local negative coupling, where the threshold density is  $\delta_c = 0.43$ . Our results conform to the constraints of current observations. Constraints are obtained from the publicly available Python code PBHbounds [65].

portant tool for studying small-scale cosmology. During the radiation dominated (RD) period, the energy density of SIGWs can be estimated using the following formula [69–71]

$$\Omega_{GW}(k, \tau_c) = \frac{1}{6} \int_0^\infty dv \int_{|1-v|}^{1+v} du \times \left[ \frac{4v^2 - (1-u^2+v^2)^2}{4uv} \right]^2 \times \overline{I_{RD}^2(u, v)} P_S(ku) P_S(kv) , \quad (23)$$

here we introduce the dimensionless variable  $v = \tilde{k}/k$  and  $u = |\mathbf{k} - \tilde{\mathbf{k}}|/k$ , The function  $\overline{I_{RD}^2(u, v)}$  in the radiation

period is defined as

$$\overline{I_{RD}^2(u, v)} = \frac{9A^2}{32u^6v^6} \left\{ \pi^2 A^2 \Theta(u + v - \sqrt{3}) + \left[ -4uv + A \ln \left| \frac{3 - (u + v)^2}{3 - (u - v)^2} \right| \right]^2 \right\}, \quad (24)$$

where we define  $A(u, v) = u^2 + v^2 - 3$  and  $\Theta$  is the Heaviside theta function. The relationship between frequency and comoving wave number can be written as

$$f = 1.546 \times 10^{-15} \left( \frac{k}{\text{Mpc}^{-1}} \right) \text{Hz}, \quad (25)$$

The current energy density of the SIGWs can be related to their value in the radiation period [71, 72]

$$\Omega_{GW,0}(k)h^2 = 0.83 \left( \frac{g_c}{10.75} \right)^{-1/3} \Omega_{r,0}h^2 \Omega_{GW}(k, \eta_c), \quad (26)$$

where  $\Omega_{r,0}h^2 \approx 4.2 \cdot 10^{-5}$  is the current radiation density parameter,  $g_c \approx 106.75$  is the effective degrees of freedom in the energy density at  $\eta_c$  [73].

In the case of positive coupling, the peak  $k_{form} \sim 10^{17} \text{Mpc}^{-1}$  corresponds to  $f \sim 10^2 \text{Hz}$ , which is high-frequency gravitational wave. In Fig. (17), we plot the SIGWs and related observation constraints of the Starobinsky potential formation in the form of local positive coupling, the peak curve lies in the allowed region of the observational constraints by the ET, CE, and NEMO results.

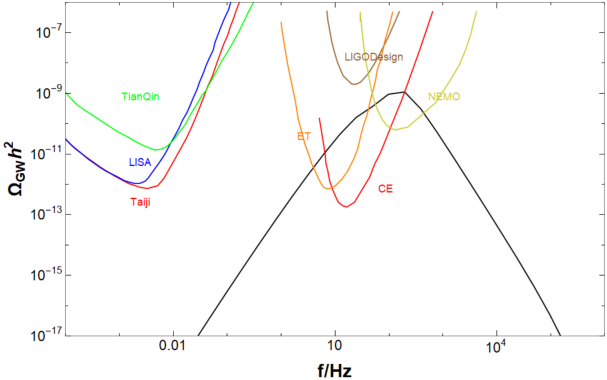


FIG. 17. The black line corresponds to the energy spectrum of SIGWs formed by the positively coupled Starobinsky potential, with parameters corresponding to Eq. (14). The colored line corresponds to the sensitivity curve of current or future GW projects [74–83].

In Fig. (18), we plot the SIGWs and related observation constraints of the Starobinsky potential formation in the form of local negative coupling, the peak  $k_{form} \sim 10^{13} \text{Mpc}^{-1}$  corresponds to  $f \sim 10^{-2} \text{Hz}$ . the peak curve lies in the allowed region of the observational constraints by the Taiji, LISA, and TianQin results. In addition, Fig. (19) corresponds to SIGWs formed by

KKLT potentials with local negative coupling, the peak corresponds to  $f \sim 7.75 \cdot 10^{-10} \text{Hz}$ . the SIGWs curve lies in the allowed region of the observational constraints by the FAST, SKA, and NANOGrav results.

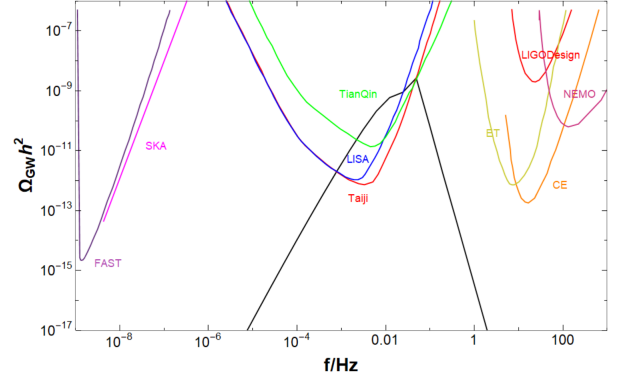


FIG. 18. The black line corresponds to the energy spectrum of SIGWs formed by the negatively coupled Starobinsky potential, with parameters corresponding to Eq. (15). The colored line corresponds to the sensitivity curve of current or future GW projects [74–83].

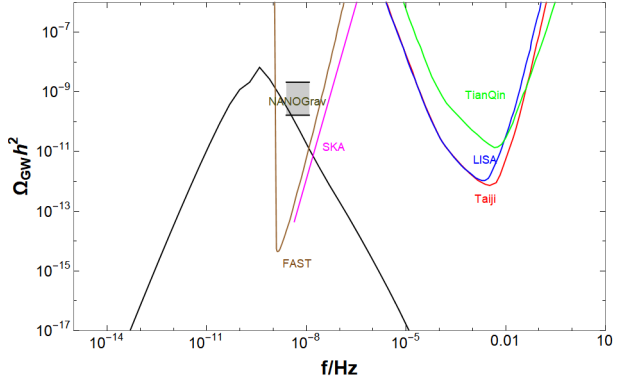


FIG. 19. The black line corresponds to the energy spectrum of SIGWs formed by the negatively coupled KKLT potential, with parameters corresponding to Eq. (17). The colored line corresponds to the sensitivity curve of current or future GW projects [74–83].

## VI. DISCUSSIONS AND CONCLUSIONS

In the paper, we studied the formation of PBHs and SIGWs with locally coupled inflation potentials. We use the Starobinsky potential and KKLT potential as the fundamental potential respectively, and apply local coupling in Lorentz form. Numerical results show that regardless of positive or negative coupling, the scalar field will transition from SR to USR, leading to the dynamic breaking of the SR parameter. Our results indicate that on the large scale, the power spectrum satisfy the observation constraints of CMB, while peaks appear in the power

spectrum on the small scale. By adjusting the parameters appropriately, the peaks can satisfy the requirements for forming the PBHs. We have separately obtained the abundance of PBHs formed by local positive coupling and local negative coupling, and the results show that their abundance is inversely proportional to the threshold density. Under the premise of satisfying current observational constraints, the PBHs formed by positive coupling may explain the formation of BBN in the early universe.

In addition, large-scale scalar perturbations on a small scale not only form PBHs, but also induce the formation of gravitational waves. We obtained SIGWs formed in two different coupling scenarios, which can be detected by current or future gravitational wave projects.

## APPENDIX

As a candidate for dark matter, PBH possess a broad mass spectrum. Within this framework, we consider the following potential form

$$V(\phi) = V_4 \phi^2 (1 \pm v_1 \pm v_2) , \quad (27)$$

where  $v_1 = \frac{B_4 C_4}{(\phi - D_4)^2 + C_4^2}$  and  $v_2 = \frac{B_5 C_5}{(\phi - D_5)^2 + C_5^2}$ . Here, we consider negative coupling “-”, the parameter  $V_4 = 1.45 \cdot 10^{-9} M_{pl}^4$  and

$$\begin{aligned} B_4 &= 4.622972 \cdot 10^{-3} M_{pl} , \quad B_5 = 3.505503 \cdot 10^{-3} M_{pl} , \\ C_4 &= 0.145 M_{pl} , \quad C_5 = 0.11 M_{pl} \\ D_4 &= 14 M_{pl} , \quad D_5 = 12 M_{pl} . \end{aligned} \quad (28)$$

As shown in Fig. (20), the coupling is located at  $\phi = 12 M_{pl}$  and  $\phi = 14 M_{pl}$ , respectively. Due to the pres-

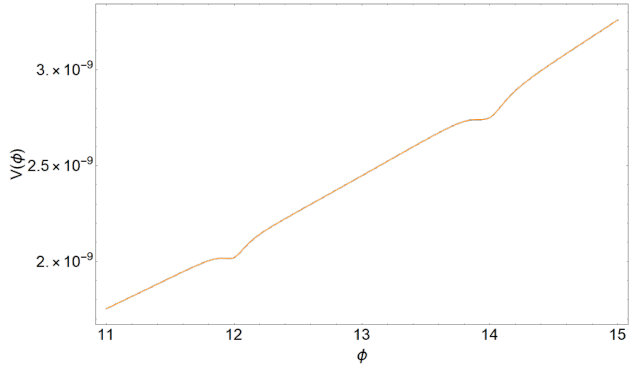


FIG. 20. The  $\phi^2$  potential with two negative coupling, and the parameter values correspond to Eq. (28), where the coupling is at  $\phi = 12 M_{pl}$  and  $\phi = 14 M_{pl}$ .

ence of double coupling, inflation undergoes two separate transitions from SR to USR regimes. Consequently, the primordial power spectrum exhibits two pronounced enhancements. Fig. (21) shows this trend, with peaks of  $2.19 \cdot 10^{-3}$  and  $9.4 \cdot 10^{-3}$  at  $k \sim 4.07 \cdot 10^5 \text{ Mpc}^{-1}$  and  $k \sim 1.818 \cdot 10^{17} \text{ Mpc}^{-1}$ , respectively. Fig. (22) presents the resulting energy spectrum of SIGWs. In principle, irrespective of whether the double coupling is positive or negative, it consistently produces two distinct enhancements in the primordial power spectrum at small scales.

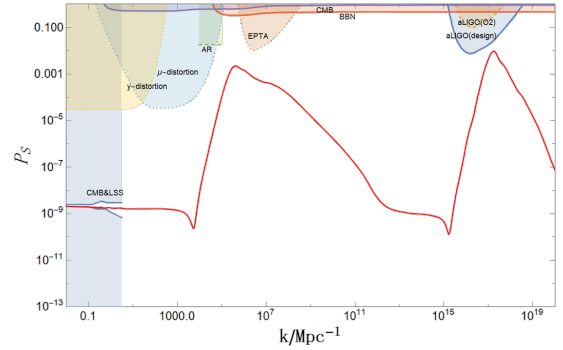


FIG. 21. The power spectrum with two negative coupling, and the parameter values correspond to Eq. (28).

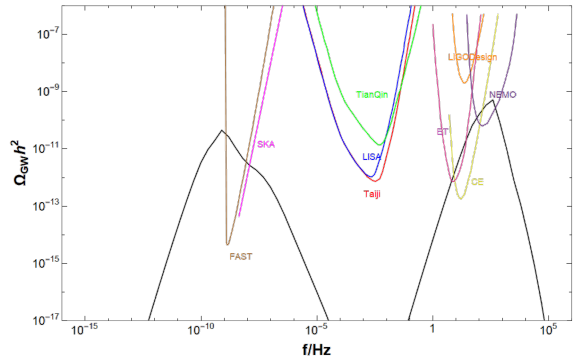


FIG. 22. The SIGWs with two negative coupling, and the parameter values correspond to Eq. (28).

---

[1] Stephen Hawking. Gravitationally collapsed objects of very low mass. *Mon. Not. Roy. Astron. Soc.*, 152:75, 1971.

[2] Bernard J. Carr and S. W. Hawking. Black holes in the early Universe. *Mon. Not. Roy. Astron. Soc.*, 168:399–415, 1974.

[3] Ya. B. Zel'dovich and I. D. Novikov. The Hypothesis of Cores Retarded during Expansion and the Hot Cosmological Model. *Sov. Astron.*, 10:602, 1967.

[4] Juan Garcia-Bellido and Ester Ruiz Morales. Primordial black holes from single field models of inflation. *Phys. Dark Univ.*, 18:47–54, 2017.

[5] Guillermo Ballesteros and Marco Taoso. Primordial black hole dark matter from single field inflation. *Phys. Rev. D*, 97(2):023501, 2018.

[6] Bernard Carr, Tommi Tenkanen, and Ville Vaskonen. Primordial black holes from inflaton and spectator field perturbations in a matter-dominated era. *Phys. Rev. D*, 96(6):063507, 2017.

[7] Shi Pi, Ying-li Zhang, Qing-Guo Huang, and Misao Sasaki. Scalaron from  $R^2$ -gravity as a heavy field. *JCAP*, 05:042, 2018.

[8] Yi-Fu Cai, Xi Tong, Dong-Gang Wang, and Sheng-Feng Yan. Primordial Black Holes from Sound Speed Resonance during Inflation. *Phys. Rev. Lett.*, 121(8):081306, 2018.

[9] Guillermo Ballesteros, Jose Beltran Jimenez, and Mauro Pieroni. Black hole formation from a general quadratic action for inflationary primordial fluctuations. *JCAP*, 06:016, 2019.

[10] Shi Pi, Misao Sasaki, and Ying-li Zhang. Primordial Tensor Perturbation in Double Inflationary Scenario with a Break. *JCAP*, 06:049, 2019.

[11] Chengjie Fu, Puxun Wu, and Hongwei Yu. Primordial Black Holes from Inflation with Nonminimal Derivative Coupling. *Phys. Rev. D*, 100(6):063532, 2019.

[12] Chao Chen and Yi-Fu Cai. Primordial black holes from sound speed resonance in the inflaton-curvaton mixed scenario. *JCAP*, 10:068, 2019.

[13] Ruifeng Zheng, Jiaming Shi, and Taotao Qiu. On primordial black holes and secondary gravitational waves generated from inflation with solo/multi-bumpy potential \*. *Chin. Phys. C*, 46(4):045103, 2022.

[14] Bernard Carr and Florian Kuhnel. Primordial black holes with multimodal mass spectra. *Phys. Rev. D*, 99(10):103535, 2019.

[15] Manuel Drees and Yong Xu. Overshooting, Critical Higgs Inflation and Second Order Gravitational Wave Signatures. *Eur. Phys. J. C*, 81(2):182, 2021.

[16] Lilia Anguelova. On Primordial Black Holes from Rapid Turns in Two-field Models. *JCAP*, 06:004, 2021.

[17] Jiong Lin, Qing Gao, Yungui Gong, Yizhou Lu, Chao Zhang, and Fengge Zhang. Primordial black holes and secondary gravitational waves from  $k$  and  $G$  inflation. *Phys. Rev. D*, 101(10):103515, 2020.

[18] Taotao Qiu, Wenyi Wang, and Ruifeng Zheng. Generation of primordial black holes from an inflation model with modified dispersion relation. *Phys. Rev. D*, 107(8):083018, 2023.

[19] Sayantan Choudhury and M. Sami. Large fluctuations and primordial black holes. *Phys. Rept.*, 1103:1–276, 2025.

[20] Sayantan Choudhury, Ahaskar Karde, Pankaj Padiyar, and M. Sami. Primordial black holes from effective field theory of stochastic single field inflation at NNNLO. *Eur. Phys. J. C*, 85(1):21, 2025.

[21] Rafid Mahbub. Primordial black hole formation in inflationary  $\alpha$ -attractor models. *Phys. Rev. D*, 101(2):023533, 2020.

[22] Amjad Ashoorioon, Abasalt Rostami, and Javad T. Firouzjaee. Examining the end of inflation with primordial black holes mass distribution and gravitational waves. *Phys. Rev. D*, 103:123512, 2021.

[23] Alexandros Karam, Niko Koivunen, Eemeli Tomberg, Ville Vaskonen, and Hardi Veermäe. Anatomy of single-field inflationary models for primordial black holes. *JCAP*, 03:013, 2023.

[24] Pasquale D. Serpico, Vivian Poulin, Derek Inman, and Kazunori Kohri. Cosmic microwave background bounds on primordial black holes including dark matter halo accretion. *Phys. Rev. Res.*, 2(2):023204, 2020.

[25] Bernard Carr, Kazunori Kohri, Yuuiti Sendouda, and Jun'ichi Yokoyama. Constraints on primordial black holes. *Rept. Prog. Phys.*, 84(11):116902, 2021.

[26] Sandeep Kumar Acharya and Rishi Khatri. CMB and BBN constraints on evaporating primordial black holes revisited. *JCAP*, 06:018, 2020.

[27] B. J. Carr, Kazunori Kohri, Yuuiti Sendouda, and Jun'ichi Yokoyama. New cosmological constraints on primordial black holes. *Phys. Rev. D*, 81:104019, 2010.

[28] Sunghoon Jung and Chang Sub Shin. Gravitational-Wave Fringes at LIGO: Detecting Compact Dark Matter by Gravitational Lensing. *Phys. Rev. Lett.*, 122(4):041103, 2019.

[29] Ranjan Laha. Primordial Black Holes as a Dark Matter Candidate Are Severely Constrained by the Galactic Center 511 keV  $\gamma$ -Ray Line. *Phys. Rev. Lett.*, 123(25):251101, 2019.

[30] Basudeb Dasgupta, Ranjan Laha, and Anupam Ray. Neutrino and positron constraints on spinning primordial black hole dark matter. *Phys. Rev. Lett.*, 125(10):101101, 2020.

[31] Rong-Gen Cai, Yu-Chen Ding, Xing-Yu Yang, and Yu-Feng Zhou. Constraints on a mixed model of dark matter particles and primordial black holes from the galactic 511 keV line. *JCAP*, 03:057, 2021.

[32] Xiu-Hui Tan, Yang-Jie Yan, Taotao Qiu, and Jun-Qing Xia. Searching for the Signal of a Primordial Black Hole from CMB Lensing and  $\gamma$ -Ray Emissions. *Astrophys. J. Lett.*, 939(1):L15, 2022.

[33] Kaze W. K. Wong, Gabriele Franciolini, Valerio De Luca, Vishal Baibhav, Emanuele Berti, Paolo Pani, and Antonio Riotto. Constraining the primordial black hole scenario with Bayesian inference and machine learning: the GWTC-2 gravitational wave catalog. *Phys. Rev. D*, 103(2):023026, 2021.

[34] Bradley J. Kavanagh, Daniele Gaggero, and Gianfranco Bertone. Merger rate of a subdominant population of primordial black holes. *Phys. Rev. D*, 98(2):023536, 2018.

[35] Rampei Kimura, Teruaki Suyama, Masahide Yamaguchi, and Ying-Li Zhang. Reconstruction of Primordial Power Spectrum of curvature perturbation from the merger rate

of Primordial Black Hole Binaries. *JCAP*, 04:031, 2021.

[36] Debottam Nandi, Rohan Roy, Simran Yadav, and Arnab Sarkar. Sub-Horizon Amplification of Curvature Perturbations: A New Route to Primordial Black Holes and Gravitational Waves. 4 2025.

[37] Daniel Baumann, Paul J. Steinhardt, Keitaro Takahashi, and Kiyotomo Ichiki. Gravitational Wave Spectrum Induced by Primordial Scalar Perturbations. *Phys. Rev. D*, 76:084019, 2007.

[38] Kishore N. Ananda, Chris Clarkson, and David Wands. The Cosmological gravitational wave background from primordial density perturbations. *Phys. Rev. D*, 75:123518, 2007.

[39] Guillem Domènech. Scalar Induced Gravitational Waves Review. *Universe*, 7(11):398, 2021.

[40] Daniel Baumann. Inflation. In *Theoretical Advanced Study Institute in Elementary Particle Physics: Physics of the Large and the Small*, pages 523–686, 2011.

[41] Misao Sasaki. Large Scale Quantum Fluctuations in the Inflationary Universe. *Prog. Theor. Phys.*, 76:1036, 1986.

[42] Viatcheslav F. Mukhanov. Quantum Theory of Gauge Invariant Cosmological Perturbations. *Sov. Phys. JETP*, 67:1297–1302, 1988.

[43] Y. Akrami et al. Planck 2018 results. X. Constraints on inflation. *Astron. Astrophys.*, 641:A10, 2020.

[44] Hayato Motohashi and Wayne Hu. Primordial Black Holes and Slow-Roll Violation. *Phys. Rev. D*, 96(6):063503, 2017.

[45] Jerome Martin, Hayato Motohashi, and Teruaki Suyama. Ultra Slow-Roll Inflation and the non-Gaussianity Consistency Relation. *Phys. Rev. D*, 87(2):023514, 2013.

[46] William H. Kinney. Horizon crossing and inflation with large eta. *Phys. Rev. D*, 72:023515, 2005.

[47] Haoran Di and Yungui Gong. Primordial black holes and second order gravitational waves from ultra-slow-roll inflation. *JCAP*, 07:007, 2018.

[48] Alexei A. Starobinsky. A New Type of Isotropic Cosmological Models Without Singularity. *Phys. Lett. B*, 91:99–102, 1980.

[49] Shamit Kachru, Renata Kallosh, Andrei D. Linde, and Sandip P. Trivedi. De Sitter vacua in string theory. *Phys. Rev. D*, 68:046005, 2003.

[50] Shamit Kachru, Renata Kallosh, Andrei D. Linde, Juan Martin Maldacena, Liam P. McAllister, and Sandip P. Trivedi. Towards inflation in string theory. *JCAP*, 10:013, 2003.

[51] Anne M. Green and Andrew R. Liddle. Constraints on the density perturbation spectrum from primordial black holes. *Phys. Rev. D*, 56:6166–6174, 1997.

[52] Misao Sasaki, Teruaki Suyama, Takahiro Tanaka, and Shuichiro Yokoyama. Primordial black holes—perspectives in gravitational wave astronomy. *Class. Quant. Grav.*, 35(6):063001, 2018.

[53] Keisuke Inomata, Masahiro Kawasaki, Kyohei Mukaida, Yuichiro Tada, and Tsutomu T. Yanagida. Inflationary Primordial Black Holes as All Dark Matter. *Phys. Rev. D*, 96(4):043504, 2017.

[54] William H. Press and Paul Schechter. Formation of galaxies and clusters of galaxies by selfsimilar gravitational condensation. *Astrophys. J.*, 187:425–438, 1974.

[55] Anne M. Green, Andrew R. Liddle, Karim A. Malik, and Misao Sasaki. A New calculation of the mass fraction of primordial black holes. *Phys. Rev. D*, 70:041502, 2004.

[56] Bernard J. Carr. The Primordial black hole mass spectrum. *Astrophys. J.*, 201:1–19, 1975.

[57] Keisuke Inomata, Masahiro Kawasaki, Kyohei Mukaida, Yuichiro Tada, and Tsutomu T. Yanagida.  $\mathcal{O}(10)M_\odot$  primordial black holes and string axion dark matter. *Phys. Rev. D*, 96(12):123527, 2017.

[58] Gabriela Sato-Polito, Ely D. Kovetz, and Marc Kamionkowski. Constraints on the primordial curvature power spectrum from primordial black holes. *Phys. Rev. D*, 100(6):063521, 2019.

[59] Ilia Musco, Valerio De Luca, Gabriele Franciolini, and Antonio Riotto. Threshold for primordial black holes. II. A simple analytic prescription. *Phys. Rev. D*, 103(6):063538, 2021.

[60] Sam Young, Christian T. Byrnes, and Misao Sasaki. Calculating the mass fraction of primordial black holes. *JCAP*, 07:045, 2014.

[61] David Blais, Torsten Bringmann, Claus Kiefer, and David Polarski. Accurate results for primordial black holes from spectra with a distinguished scale. *Phys. Rev. D*, 67:024024, 2003.

[62] Sam Young. The primordial black hole formation criterion re-examined: Parametrisation, timing and the choice of window function. *Int. J. Mod. Phys. D*, 29(02):2030002, 2019.

[63] Koki Tokeshi, Keisuke Inomata, and Jun’ichi Yokoyama. Window function dependence of the novel mass function of primordial black holes. *JCAP*, 12:038, 2020.

[64] S. W. Hawking. Black hole explosions. *Nature*, 248:30–31, 1974.

[65] Bradley J. Kavanagh. bradkav/pbhbounds: Release version, November 2019.

[66] Peter W. Graham, Surjeet Rajendran, and Jaime Varela. Dark Matter Triggers of Supernovae. *Phys. Rev. D*, 92(6):063007, 2015.

[67] A. Barnacka, J. F. Glicenstein, and R. Moderski. New constraints on primordial black holes abundance from femtolensing of gamma-ray bursts. *Phys. Rev. D*, 86:043001, 2012.

[68] Fabio Capela, Maxim Pshirkov, and Peter Tinyakov. Constraints on primordial black holes as dark matter candidates from capture by neutron stars. *Phys. Rev. D*, 87(12):123524, 2013.

[69] Rong-gen Cai, Shi Pi, and Misao Sasaki. Gravitational Waves Induced by non-Gaussian Scalar Perturbations. *Phys. Rev. Lett.*, 122(20):201101, 2019.

[70] Milad Solbi and Kayoomars Karami. Primordial black holes formation in the inflationary model with field-dependent kinetic term for quartic and natural potentials. *Eur. Phys. J. C*, 81(10):884, 2021.

[71] Pisin Chen, Seoktae Koh, and Gansukh Tumurtushaa. Primordial black holes and induced gravitational waves from inflation in the Horndeski theory of gravity. 7 2021.

[72] Shi Pi and Misao Sasaki. Gravitational Waves Induced by Scalar Perturbations with a Lognormal Peak. *JCAP*, 09:037, 2020.

[73] Lars Husdal. On Effective Degrees of Freedom in the Early Universe. *Galaxies*, 4(4):78, 2016.

[74] Rendong Nan, Di Li, Chengjin Jin, Qiming Wang, Lichun Zhu, Wenbai Zhu, Haiyan Zhang, Youling Yue, and Lei Qian. The Five-Hundred-Meter Aperture Spherical Radio Telescope (FAST) Project. *Int. J. Mod. Phys. D*, 20:989–1024, 2011.

- [75] Gemma Janssen et al. Gravitational wave astronomy with the SKA. *PoS*, AASKA14:037, 2015.
- [76] Jun Luo et al. TianQin: a space-borne gravitational wave detector. *Class. Quant. Grav.*, 33(3):035010, 2016.
- [77] Jianwei Mei et al. The TianQin project: current progress on science and technology. *PTEP*, 2021(5):05A107, 2021.
- [78] Pau Amaro-Seoane et al. Laser Interferometer Space Antenna. 2 2017.
- [79] Wen-Rui Hu and Yue-Liang Wu. The Taiji Program in Space for gravitational wave physics and the nature of gravity. *Natl. Sci. Rev.*, 4(5):685–686, 2017.
- [80] K. Ackley et al. Neutron Star Extreme Matter Observatory: A kilohertz-band gravitational-wave detector in the global network. *Publ. Astron. Soc. Austral.*, 37:e047, 2020.
- [81] S. Hild et al. Sensitivity Studies for Third-Generation Gravitational Wave Observatories. *Class. Quant. Grav.*, 28:094013, 2011.
- [82] Benjamin P Abbott et al. Exploring the Sensitivity of Next Generation Gravitational Wave Detectors. *Class. Quant. Grav.*, 34(4):044001, 2017.
- [83] B. P. Abbott et al. Search for the isotropic stochastic background using data from Advanced LIGO’s second observing run. *Phys. Rev. D*, 100(6):061101, 2019.